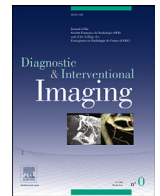




ELSEVIER



Original article

Research, New developments & Artificial Intelligence

Gadolinium K-edge angiography with a spectral photon counting CT in atherosclerotic rabbits

Sara Boccalini^{a,b,*}, Riham Dessouky^{c,d}, Pierre-Antoine Rodesch^c, Hugo Lacombe^c, Yoad Yagil^e, Elias Lahoud^e, Klaus Erhard^f, Bernhard Brendel^f, Philippe Coulon^g, Jean-Baptiste Langlois^h, Frederic Chaputⁱ, Stephane Parolaⁱ, Loic Bousset^{b,c}, Frederic Lerougeⁱ, Salim Si-Mohamed^{b,c}, Philippe C. Douek^{b,c}

^a Lyon University, Université Claude Bernard Lyon 1, 69100 Villeurbanne, France

^b Department of Cardiovascular and Thoracic Radiology, Louis Pradel Hospital, Hospices Civils de Lyon, 69500 Bron, France

^c Lyon University, INSA-Lyon, Université Claude Bernard Lyon 1, UJM-Saint Etienne, CNRS, INSERM, CREATIS UMR 5220, U1206, 69100 Villeurbanne, France

^d Department of Radiology, Faculty of Medicine, Zagazig University, 44519, Zagazig, Egypt

^e Philips Medical Systems, 31004 Haifa, Israel

^f Philips Research, 22335 Hamburg, Germany

^g Philips Healthcare, 92156 Suresnes, France

^h CERMEP Centre d'Imagerie du Vivant, 69500 Bron, France

ⁱ Laboratoire de Chimie, Université de Lyon, École Normale Supérieure de Lyon, Université Claude Bernard Lyon 1, CNRS UMR 5182, 69364 Lyon, France

ARTICLE INFO

Keywords:

CT-angiography

Gadolinium based contrast agent

K-edge imaging

Spectral photon counting CT

ABSTRACT

Purpose: The purpose of this study was to investigate the feasibility of gadolinium-K-edge-angiography (angio-Gd-K-edge) with gadolinium-based contrast agents (GBCAs) as obtained with spectral photon counting CT (SPCCT) in atherosclerotic rabbits.

Materials and methods: Seven atherosclerotic rabbits underwent angio-SPCCT acquisitions with two GBCAs, with similar intravenous injection protocol. Conventional and angio-Gd-K-edge images were reconstructed with the same parameters. Regions of interest were traced in different locations of the aorta and its branches. Hounsfield unit values, Gd concentrations, signal-to-noise (SNR) and contrast-to-noise (CNR) were calculated and compared. The maximum diameter and the diameter of the aorta in regard to atherosclerotic plaques were measured by two observers. Images were subjectively evaluated regarding vessels' enhancement, artefacts, border sharpness and overall image quality.

Results: In the analyzable six rabbits, Gd-K-edge allowed visualization of target vessels and no other structures. HU values and Gd concentrations were greatest in the largest artery (descending aorta, 5.6 ± 0.8 [SD] mm), and lowest in the smallest (renal arteries, 2.1 ± 0.3 mm). While greater for conventional images, CNR and SNR were satisfactory for both images (all $P < 0.001$). For one observer there were no statistically significant differences in either maximum or plaque-diameters ($P = 0.45$ and all $P > 0.05$ in post-hoc analysis, respectively). For the second observer, there were no significant differences for images reconstructed with the same parameters (all $P < 0.05$). All subjective criteria scored higher for conventional images compared to K-edge (all $P < 0.01$), with the highest scores for enhancement ($4.3-4.4$ vs. $3.1-3.4$).

Conclusion: With SPCCT, angio-Gd-K-edge after injection of GBCAs in atherosclerotic rabbits is feasible and allows for angiography-like visualization of small arteries and for the reliable measurement of their diameters.

© 2023 Published by Elsevier Masson SAS on behalf of Société française de radiologie.

Abbreviations: CNR, Contrast to noise ratio; CT, Computed tomography; DA, Diaphragmatic aorta; DMA, Distal superior mesenteric artery; DTA, Descending thoracic aorta; GBCA, Gadolinium based contrast agent; L-DRA, Left distal renal artery; L-PRA, Left proximal renal artery; MRI, Magnetic resonance imaging; PMA, Proximal superior mesenteric artery; R-DRA, Right distal renal artery; R-PRA, Right proximal renal artery; SNR, Signal-to-noise ratio; SPCCT, Spectral photon counting CT

* Corresponding author.

E-mail address: sara.boccalini@chu-lyon.fr (S. Boccalini).

<https://doi.org/10.1016/j.diii.2023.05.002>

2211-5684/© 2023 Published by Elsevier Masson SAS on behalf of Société française de radiologie.

1. Introduction

Non-invasive imaging of arteries, with computed tomography (CT) or magnetic resonance imaging (MRI), has become the reference for the assessment of most anatomic regions, from the intracranial to the plantar arteries. Besides some location-specific peculiarities, in particular the coronary arteries that require electrocardiogram

synchronization, some common limitations are systematically encountered. First, small vessels are difficult or impossible to accurately assess as they are at (or below) the limit of spatial resolution of clinical systems. Second, calcifications, bones and dense artificial materials are limitations for CT examinations [1,2]. Indeed, not only they hamper the correct assessment of stenosis due to blooming artifacts but, especially in very small vessels, they are often indistinguishable from enhanced lumen making even the basic judgment of vascular patency unachievable. Third, regardless of the imaging modality employed, administration of contrast material is generally required and elicits well-known concerns [3].

MRI can overcome some of these limitations thanks to angiographic sequences with background suppression and sequences capable of revealing arterial lumen without the need for using contrast material. However, MRI examinations are sparsely available, expensive, and time-consuming. In addition, the above-mentioned sequences are prone to several pitfalls and of limited use for regions other than intracranial vessels [4].

On the contrary, spectral photon counting CT (SPCCT) has the potential to overcome these limitations by combining all the advantages of CT with its new features. With these revolutionary scanners, spatial resolution is greatly improved, and blooming artifacts are reduced, for instance in coronary arteries [5,6]. Furthermore, as photons are directly counted and classified in specific energy bins, SPCCT allows for the so-called “K-edge imaging.” This technique relies on the specific depiction of certain elements [7]. The prerequisite is that the K-edge of the element of interest needs to fall in the range of energy values that can be explored with SPCCT. Therefore, the list of depictable materials includes gadolinium but not iodine that has its K-edge at 33 keV, too low to be imaged with SPCCT. Therefore, following injection of gadolinium in the circulation system of a living creature, K-edge imaging enables visualization (and quantification) of this sole element, hence only the enhanced vascular lumina, in a purely angiographic image.

The purpose of this study was to investigate the feasibility of K-edge angiography after different gadolinium-based contrast agents (GBCA) injection in atherosclerotic rabbits with a SPCCT prototype.

2. Materials and methods

2.1. Animals

Between May 2019 and July 2019, seven rabbits were included. They were seven male New Zealand white rabbits (Charles River) of 3.4 ± 0.1 (standard deviation [SD]) kg (range: 3.3–3.5 kg) were fed a controlled diet and underwent interventional procedures on the aorta, as previously described [8]. All procedures were conducted in accordance with the European Directive 2010/63/UE, approved by the Ethics Committee and authorized by the French Ministry of Higher Education, Research and Innovation (APAFIS#27330). All experiments were performed after specific approval from the Institutional Animal Care and Use Committee (CELYNE committee, APAFIS#1732-2015091411181645). These procedures promote atherosclerotic plaques, calcifications, and aneurysms development in the aorta.

2.2. Injection protocol

Three rabbits received intravenous administration of gadoteridol (ProHance®, Bracco Imaging) and four received intravenous administration of PEGylated nanoparticles with a 14 nm hydrodynamic diameter (GdF³⁺) [9]. Two of them received intravenous administration of both contrast materials, gadoteridol first and GdF³⁺ two months later.

Five mL/kg of GBCA were injected at 2 mL/s via a vein in the ear of the rabbit, followed by a flush of 2 mL of saline at 0.5 mL/s. The dose was 0.5 mmol/mL for both GBCAs, with matching total numbers of

atoms of Gd. The total injected volume per scan was 17.4 ± 0.6 (SD) mL (range: 17–18 mL). Acquisitions were performed eight seconds after the start of the administration of contrast material in all rabbits.

2.3. SPCCT acquisition and reconstruction parameters

After contrast material injection, arterial acquisitions were performed with a prototype of SPCCT. Both conventional and gadolinium K-edge (Gd-K-edge) images were reconstructed and analyzed. The SPCCT system was a clinical prototype with a large field-of-view (500 mm in-plane) featuring energy-sensitive photon-counting detectors of 2-mm-thick cadmium zinc telluride, bonded to Philips' proprietary ChromAIX2 application-specific integrated circuit [10]. The pixel dimensions at isocenter were of $270 \times 270 \mu\text{m}^2$. This system allowed the configuration of five controllable energy thresholds that were set at 30, 51, 64, 72 and 85 keV for optimized image quality on gadolinium enhanced images for the purposes of this study.

Conventional and Gd-K-edge images were reconstructed with the same parameters (field of view, 256; matrix, 1024; slice thickness, 0.5 mm) using one reconstruction kernel for conventional images and two for K-edge, with and without hybrid iterative reconstruction.

The current full spectral image chain follows a two-step approach for spectral reconstruction, based on published data and as previously reported [7,11]. A three-material basis was employed for this study comprising water-calcium-gadolinium.

Acquisition and reconstruction parameters are shown in Table 1. An example of the six reconstructions employed in this study is showed in Fig. 1.

2.4. Objective image quality assessment

2.4.1. Visualization of target vessels and identification of landmarks

As a preliminary step, visibility of vessels at predefined landmarks on the different reconstructions was assessed and their diameter measured. Furthermore, the presence of detectable vessels <1 mm was recorded. The chosen landmarks were: (i), descending thoracic aorta (at the level of the pulmonary arteries; DTA); (ii), descending aorta (at diaphragm; DA); (iii), infrarenal aorta; (iv), proximal renal

Table 1
Spectral photon counting CT acquisition and reconstruction parameters.

Parameters	Values
Acquisition	
kVp	120
mA	200
Scanning length (mm)	240
Rotation time (s)	0.75
Pitch	1.027
CTDI (mGy)	14.7
DLP (mGy cm)	513.4
Energetic bin levels (keV)	30, 51, 64, 72 and 85
Reconstruction	
Field of view (mm)	256
Matrix	1024
Binning ^a	1 × 2
Slice thickness (mm)	0.5
Kernel	Conventional: Detailed; K-edge: soft + detailed
Iterative reconstruction	FBP + iDose3 for conv

CTDI, CT dose index; DLP, dose length product; FBP, filter back projection.

^a The term “binning” and its specifications (in this case 1 × 2) define the number of original pixels of the photon counting detectors that are combined to obtain the final output of the pixel-unit.

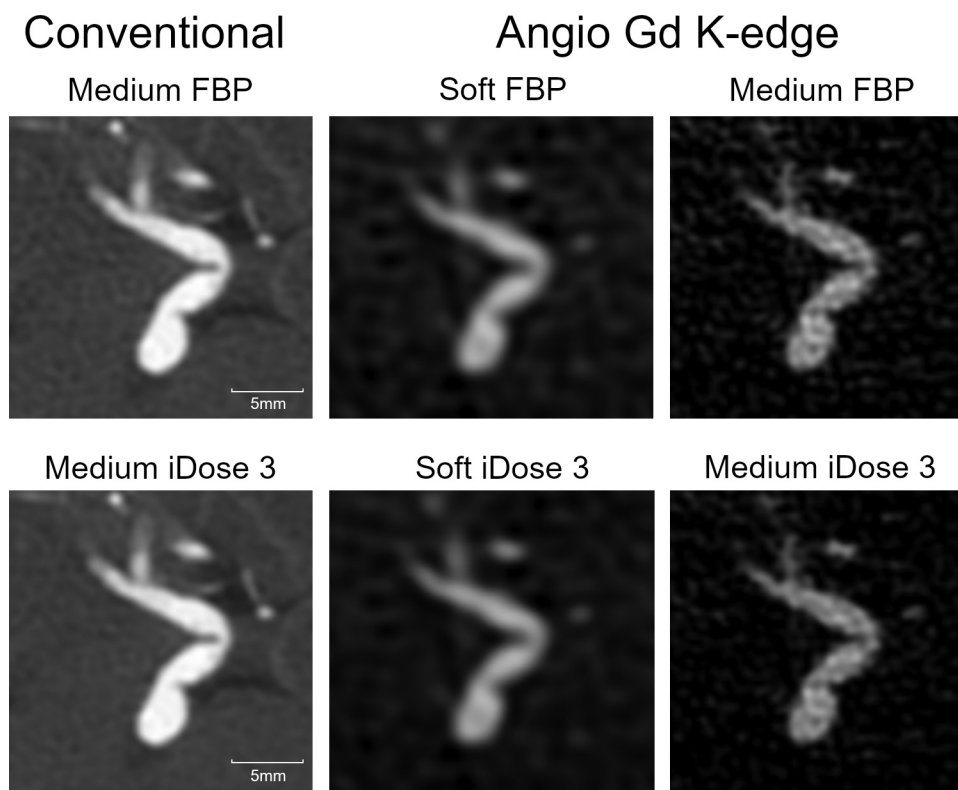


Fig. 1. Example of all the assessed reconstructions for conventional and angio-Gd-K-edge images at the level of the celiac trunk of a rabbit. The diameter of the aorta at this level is 3.5 mm. The smallest visible vessel is of about 0.4 mm of diameter on conventional images and 0.8 mm on K-edge.

arteries (5 mm after the ostium; R-PRA and L-PRA for the right and left, respectively); (v), distal renal arteries (before the division; R-DRA, L-DRA); (vi), proximal superior mesenteric artery (1 cm from origin; PMA); and (vii), distal superior mesenteric artery (4 cm from origin; DMA).

2.4.2. Hounsfield unit and gadolinium concentration values

Regions of interest (ROI) were drawn on conventional and Gd-K-edge images at the above-mentioned specific landmarks. Circular ROIs, as large as possible without overlapping with the vessels' wall, were drawn on three consecutive slices for each landmark and in paravertebral muscles. For each ROI, Hounsfield unit (HU) values, Gd content in mg/mL and their standard deviation (SD) were recorded for conventional and K-edge images, respectively. The average of the three ROIs values was used for further analysis.

2.4.3. Noise, signal-to-noise and contrast-to-noise ratios

SD values of HU on conventional images and of gadolinium concentration on K-edge images were used as measures of noise.

Signal-to-noise ratio (SNR) and contrast-to-noise ratio (CNR) were calculated as follows: (i), $SNR-HU = \text{vascular HU} / \text{vascular SD}$; (ii), $SNR-Gd = \text{vascular Gd [mg/mL]} / \text{vascular SD [mg/mL]}$; (iii), $CNR-HU = (\text{vascular HU} - \text{muscular HU}) / \text{vascular SD}$; and (iv), $CNR-Gd = (\text{vascular Gd [mg/mL]} - \text{muscular Gd [mg/mL]}) / \text{vascular SD [mg/mL]}$.

2.5. Measurements of aortic diameters at specific locations

Predefined levels of the aorta corresponding to the presence of atherosclerotic plaques were selected beforehand by an experienced radiologist. Then, two radiologists with nine and 10 years of experience in cardiovascular imaging (R.D. and S.B., respectively) independently measured the maximum diameter and the diameter obtained

going from a point on the inner border of the wall of the aorta corresponding to the middle of the plaque to the opposite side of the vessel (plaque-diameter). Measurements were performed on axial images for reconstructions with Detailed kernel for conventional images and for each of the available reconstructions for K-edge images. To ensure comparable measures on both types of images, the technique described in Fig. 2 was employed.

2.6. Subjective image quality assessment

The two observers independently scored images at each of the above-mentioned landmarks regarding vascular enhancement, artefacts, sharpness of the borders and overall image quality for all available reconstructions of both conventional and K-edge images. For each parameter, a 5-point Likert scale was used: 1, uninterpretable: absent opacification/extremely severe artifacts/impossible to distinguish the vessel borders/no diagnostic conclusion possible; 2, poor: insufficient opacification/major artifacts/difficult to distinguish the vessel borders/images difficult to interpret, non-diagnostic; 3, acceptable: sufficient opacification/modest artifacts/distinguishable vessel borders/sufficient for diagnostic purposes with limited confidence; 4, good: good opacification/negligible artifacts/well defined vessel borders/diagnostic image quality with good confidence; 5, excellent: perfect opacification/no artifacts/sharply defined borders/ diagnostic image quality with strong confidence.

2.7. Statistical analysis

Statistical analyses were performed with SPSS version 21.0 (IBM Corporation). Continuous variables were reported as means \pm SDs or medians and interquartile ranges (Q1, Q3) depending on their distributions [12]. Analysis of variance (ANOVA) for repeated measures with Bonferroni correction was used to compare HU values,

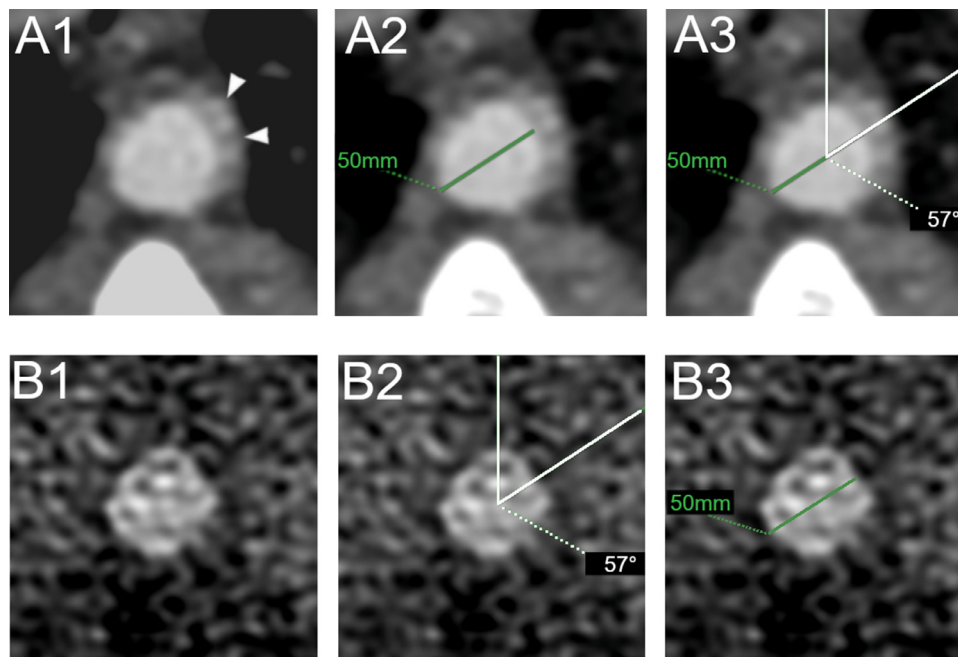


Fig. 2. Method to measure aortic diameters in regard to atherosclerotic plaques. To ensure comparable measurements between conventional and K-edge images, the angle of the measurement line on conventional images where the plaques were visible was recorded for further use. In fact, as plaques were not necessarily causing a stenosis and, by definition, were not visible on K-edge imaging, whenever in doubt observers could use the recorded angle as a guide. Details of each undertaken step are as follows: on conventional images the plaque is visible on the predefined slices (A1, arrowheads) and the diameter can be measured as in clinical practice (A2); the angle between conventional 12 h and the line used for the measurement is then recorded (angle between the two white lines, A3); on the angio-Gd-K-edge the plaque is not visible (B1); therefore, to be reproducible, the angle defined on the conventional image is transposed on the K-edge (B2) and then the measurement can be performed on the so identified plane (B3).

gadolinium concentrations, noise levels, SNR and CNR values. ANOVA for repeated measures was used to assess differences between vessels' diameters.

3. Results

Images of one rabbit were of very bad quality due to motion artefacts and bad injection timing resulting in almost absent vascular enhancement, and were therefore disregarded. This resulted in a total of six rabbits available for further analysis, including three who received gadoteridol and three who received GdF³⁺.

3.1. Visualization of target vessels, plaques, and vessels' diameters

All target vessels were clearly identifiable on both conventional and K-edge images.

In all rabbits, vessels with diameters <1 mm could be visualized on both type of images. On K-edge images, only the lumina of the vessels and organs with diffuse early enhancement (namely the lungs and the kidneys) were visible (Fig. 3). Furthermore, on K-edge images, as the bones were not visible, all vessels passing next to them or inside bony canals were well depicted (Fig. 4). Calcified atherosclerotic plaques were visible on conventional images. Since only the vessels' lumina were visible, none of the plaques was detectable on K-edge images (Fig. 5).

Mean diameters of analyzed vessels are reported in Table 2. The largest vessel was the descending aorta (5.6 ± 0.8 [SD] mm) and the smallest was the distal right renal artery (2.1 ± 0.3 [SD] mm).

3.2. Objective image quality assessment

3.2.1. Hounsfield unit and gadolinium concentration values

Mean HU and gadolinium values are reported in Table 2 per vessel and in Table 3 per reconstruction parameter. With HU values in the range of 538–647, enhancement in the vessels of the rabbits

was very good. Differences in HU between vessels were significant ($P = 0.04$) with the greatest values in the diaphragmatic aorta and the lowest in the right distal renal artery. Also, gadolinium concentrations were different between vessels ($P = 0.007$) with the highest concentration found in the diaphragmatic aorta (9.9 mg/mL), in accordance to the high HU values, and the lowest in the left proximal renal artery (7.3 mg/mL).

For K-edge images, gadolinium concentration was greatest with the Soft iDose 3 reconstruction. In addition, only the pair Soft iDose 3 vs. Detailed iDose 3 was significantly different ($P = 0.018$). Correlation

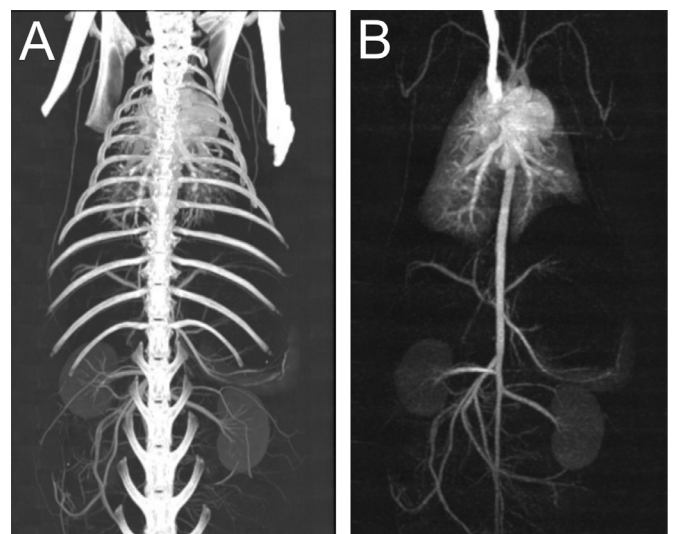


Fig. 3. Conventional (A) and angio-Gd-K-edge (B) coronal MIP reconstruction of a rabbit of 3.5 kg injected with gadoteridol. On conventional images in A all the skeleton of the rabbit is visible while, as expected, no bones are visible on the angio-Gd-K-edge image (B). The lung, the kidneys and the spleen are visible in B as they are already perfused by the Gd based contrast media.

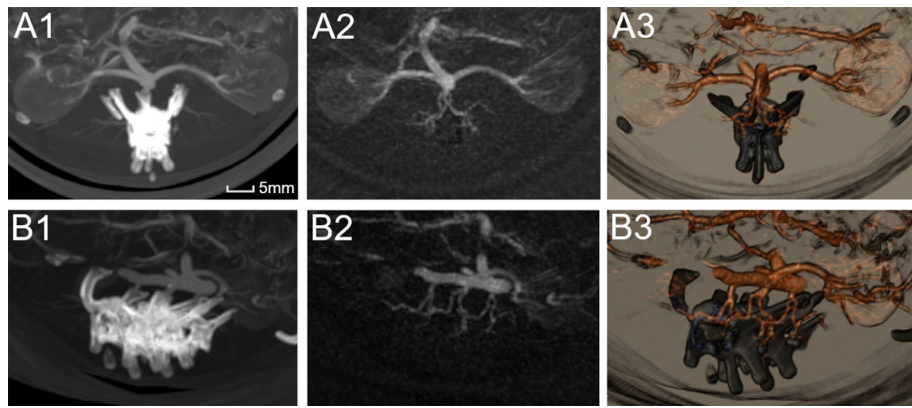


Fig. 4. Axial (A) and modified sagittal (B) MIP (A1–2, B1–2) of conventional (A1, B1) and angio-K-edge (A2, B2) reconstructions and fused volume rendering (A3, B3) of a rabbit of 3.3 kg injected with gadoteridol. On A1–B1 the vertebral and paravertebral arteries are not assessable due to the presence of the vertebrae. On A2–B2 all these arteries are clearly visible and potentially assessable as only the vascular lumina filled with Gd are visible. Volume rendering images (A3 and B3) were obtained fusing the two datasets, the conventional images for the bones and the K-edge images for the vessels. As the two datasets are actually from the same acquisition, there is a perfect matching allowing perfect fusion and leaving the operator free to change fusion parameters, such as the relative contribution of the two datasets, depending on the final desired use of the rendering.

between HU and gadolinium concentrations was very good and is shown in Fig. 6.

3.2.2. Noise, contrast-to-noise and signal-to-noise ratio

Values of noise, CNR and SNR per reconstruction parameter are reported in Table 3.

The use of iDose 3 resulted in reduced noise for Detailed kernel for conventional images (14%; $P = 0.001$) and for K-edge images for both kernels (7% and 14%, respectively; both $P < 0.001$). K-edge images with Soft filter showed reduced noise compared to the ones with Detailed filter ($P < 0.001$).

SNR and CNR values were significantly greater for conventional than for K-edge images ($P < 0.001$). For Gd-K-edge, iDose 3 reconstructions yielded significantly greater values. Soft filter resulted in almost doubled values of SNR and CNR (all $P < 0.001$).

3.3. Measurements of aortic diameters at specific locations

Measurements from the first observer did not show significant differences in maximum diameter assessment for the six available reconstructions ($P = 0.45$). For plaque-diameters, the overall difference was significant ($P = 0.04$) but pairwise comparisons after Bonferroni correction did not show any differences.

For the other observer, differences were significant for maximum diameters ($P < 0.001$) and for plaque-diameters ($P = 0.001$). For maximum diameters the greatest difference was 0.4 mm between K-edge Soft FBP and Detailed iDose 3 reconstructions ($P < 0.001$) and the smallest was 0.01 mm between Detailed iDose 3 conventional images and Detailed FBP K-edge images ($P > 0.99$). For plaque-diameters, the largest difference was 0.3 mm between Detailed FBP conventional and Detailed iDose 3 K-edge reconstructions ($P < 0.001$) and the smallest of 0.003 mm between conventional Detailed filter (both FBP and iDose 3) and Detailed iDose 3 K-edge reconstructions ($P > 0.99$). However, both maximum and plaque diameters differences between the same reconstructions of conventional and K-edge images did not show significant differences (all $P < 0.05$).

Bland Altman plots for reconstructions with Detailed kernel for maximum and plaque diameters for the two observers are reported in Fig. 7.

3.4. Subjective image quality

Subjective image quality was better for conventional for all evaluated criteria regardless of reconstruction parameters (all $P < 0.001$). The parameter receiving the highest scores was the enhancement of

the vessels that was considered acceptable to good for K-edge (overall: 3.3 ± 1.2 [SD]; range of the different types of reconstructions: 3.1–3.4) and good to excellent for conventional images (overall: 4.4 ± 0.7 ; range of the different types of reconstructions: 4.3–4.4). Sharpness of vessel borders was the parameter that was assigned the lowest score, judged poor to acceptable for K-edge (overall: 2.5 ± 0.9 [SD]; range of the different types of reconstructions: 2.4–2.5) and acceptable to good for conventional images (overall: 3.5 ± 0.5 ; range of the different types of reconstructions: 3.2–3.8). Artifacts were considered more pronounced on the K-edge images (2.7 ± 1.0 [SD]) than on conventional images (4.2 ± 0.6 [SD]).

For overall image quality, the five scores had the following distribution for K-edge compared to conventional images: 16.8% vs. 0% for 1; 17.8% vs. 0% for 2; 28% vs. 24.3% for 3; 37% vs. 70% for 4; and 0% vs. 5.6% for 5, respectively. Fifty-six p. cent of the total had an overall score ≥ 4 and 82.7% ≥ 3 .

For K-edge images, the only parameter that showed significant differences between Soft vs. Detailed filter was the sharpness of the borders.

4. Discussion

In atherosclerotic rabbits receiving GBCAs, SPCCT enabled the reconstruction of angiographic gadolinium K-edge images that allowed depiction of the lumina of small and very small (even <1 mm) arteries and no other tissue around. Although objective parameters and subjective scores of K-edge images were inferior compared to conventional images, the diameters of the vessels larger than 2 mm, including the diameters in regard to atherosclerotic plaques, could be calculated on both type of images with similar results.

PCCT is a recently introduced CT technology that has shown very promising results and is regarded by many as the future of CT. The novelty of these systems relies on the characteristics of the detectors that allow for direct transformation of photons in electric signal, a process more effective than using energy-integrating detectors [5]. These features translate into improved spatial resolution, less electronic noise and artifacts, especially blooming, on conventional images. Indeed, all these properties have been verified in humans for imaging of arteries of the neck [13,14], lung [15] as well as for coronary arteries, coronary stents and coronary calcifications [5,6]. In this study, we further confirmed previous results as we found that even submillimetric vessels can be visualized with SPCCT.

Besides all these improvements, SPCCT, thanks to the direct photon counting and attribution of photons to multiple energetic bins, is

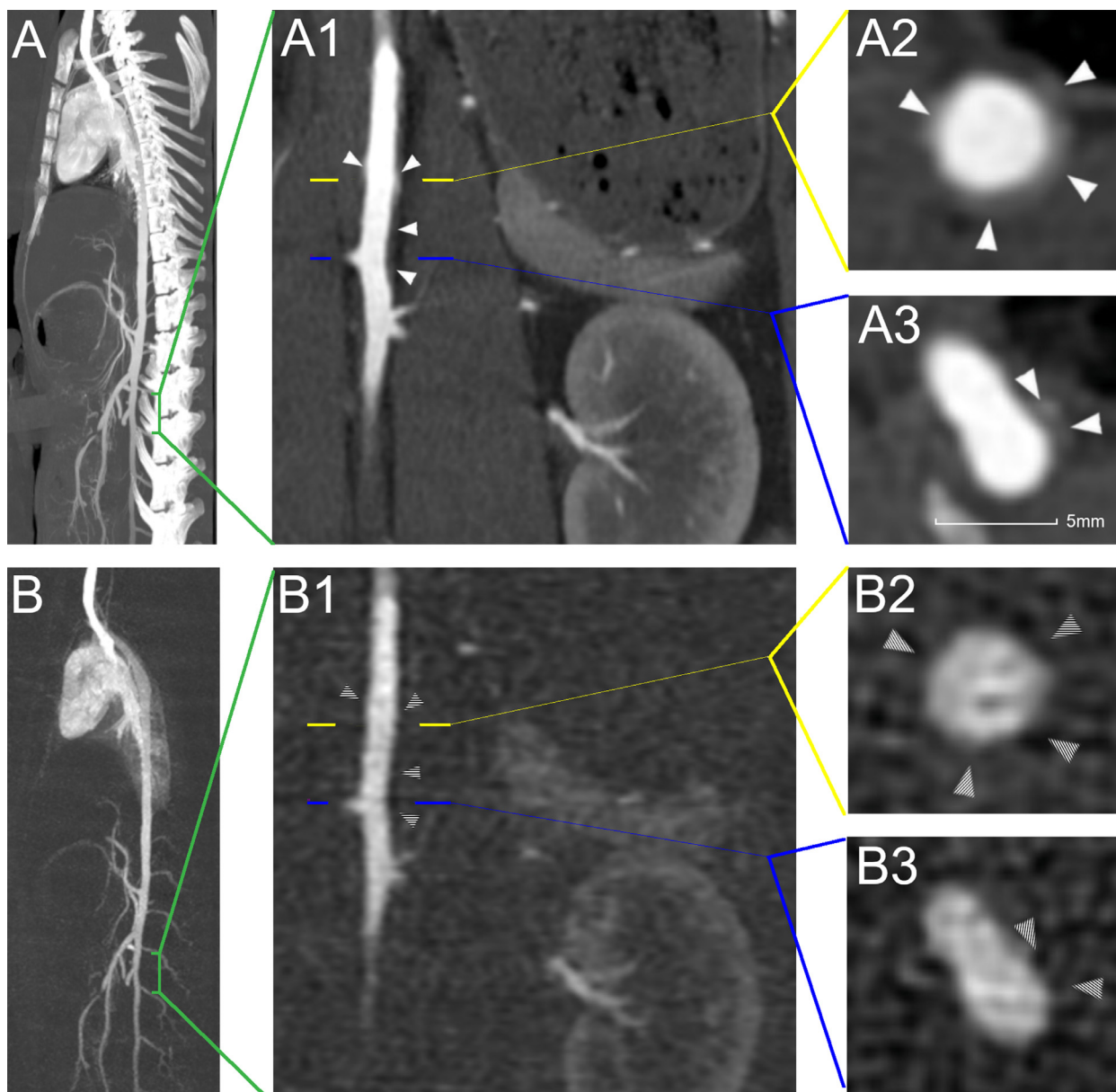


Fig. 5. Conventional (A) and angio-Gd-K-edge (B) sagittal MIP images of the same rabbit of Fig. 2. Coronal conventional (A1) and angio-Gd-K-edge (B) zooms on the abdominal aorta of the rabbit showing diffuse atherosclerotic plaques, partially calcified, of the aorta visible only on the conventional image (arrowheads in A1 and striped arrowheads in B1). In addition, a mildly dilated portion of the aorta can be noticed at the level of the first arrowheads. Cross sectional images of the aorta, corresponding to the yellow and blue lines in A1 and B1, are provided in A2-A3 (conventional images with Detailed iDose 3) and B2-B3 for Gd-K-edge images. Notice how atherosclerotic lesions of the aortic wall and its branch are visible only on conventional images (arrowheads in A2-A3 and striped arrowheads in B2-B3) and only the lumen of the vessels is visible on angio-Gd-K-edge images.

expected to provide not only better spectral resolution than dual-energy CT based on energy-integrating detectors but also new types of imaging such as K-edge imaging [6,16]. Elements have a spike in their attenuation spectrum, corresponding to the value of the bounding energy of the K-shell electron of the atom. This energy is detectable by SPCCT if comprised within the range of energies used for clinical imaging ($\approx 40\text{--}140$ keV). Thereafter, this information can be translated into images featuring the presence (and concentration) of the sole element with that specific K-edge peak [7].

In our study, we took advantage of these properties of SPCCT to obtain angio-Gd-K-edge images in rabbits. As expected, on these images only the vascular lumina were visible as they were enhanced by GBAs thereby providing purely angiographic images. This is an extremely interesting result and an advancement in CT technology that could profoundly affect clinical applications. The interest in angiographic images is longstanding and lays its roots in the

improved visualization of lumina with background suppression and better estimation of vessel patency, stenosis, components of atherosclerotic plaque and differentiation of contrast media from surgical material [17–19]. Due to these purported advantages, several post-processing tools have been developed for CT images aiming at either reducing or eliminating blooming artifacts of calcifications and other dense structures like stents [20–22]. Nevertheless, these techniques are prone to errors due to the necessary post-processing manipulations and, perhaps even more importantly, they generally require two acquisitions to subtract images, thus increasing the radiation dose. Dual-energy CT is a potentially interesting tool as it is theoretically capable of separating calcifications from iodine due to the differences in their attenuation spectra [23]. However, the separation of these materials is not perfect, relies on several assumptions and its precision varies for instance depending on the respective densities of the two materials [24]. Contrary to all these techniques, with K-edge

Table 2

Vessel diameters and average Hounsfield unit, gadolinium concentration and noise per vessel.

Arteries	Diameter [mm]	Conventional		K-edge gadolinium	
		HU ^a	Noise ^a	Gd [mg/mL] ^a	Noise ^a
DTA	5.6 ± 0.8	537 ± 180	27.6 ± 5.0	7.8 ± 3.1	1.3 ± 0.6
DA	5.0 ± 0.6	647 ± 287	27.7 ± 10.6	9.9 ± 4.7	1.4 ± 0.7
IA	3.5 ± 0.4	595 ± 252	28.5 ± 14.6	8.6 ± 4.4	1.4 ± 0.6
R-PRA	2.7 ± 0.8	569 ± 267	30.8 ± 19.3	9.1 ± 4.7	1.9 ± 1.1
L-PRA	2.5 ± 0.2	546 ± 238	26.4 ± 16.2	7.3 ± 3.7	1.3 ± 0.6
R-DRA	2.1 ± 0.3	528 ± 248	32.0 ± 12.7	8.1 ± 4.6	1.4 ± 0.5
L-DRA	2.5 ± 0.3	548 ± 204	32.1 ± 18.1	8.1 ± 3.3	1.3 ± 0.4
PMA	3.3 ± 0.4	600 ± 290	23.7 ± 11.4	8.6 ± 4.3	1.4 ± 0.6
DMA	2.7 ± 0.6	550 ± 262	25.8 ± 9.6	7.9 ± 4.0	1.3 ± 0.6

^a Mean of values from different reconstructions with corresponding standard deviation. DA: diaphragmatic aorta; DMA, distal superior mesenteric artery; DTA, descending thoracic aorta; Gs, gadolinium; IA, infrarenal aorta; L-DRA, right distal renal artery; L-PRA, left proximal renal artery; PMA, proximal superior mesenteric artery; R-DRA, right distal renal artery; R-PRA, right proximal renal artery.

imaging, data about the target material is acquired directly and specifically from the detectors.

Furthermore, our results showed that on angio-Gd-K-edge images, diameters of the vessels (both maximum and plaque-diameters) can be calculated with good accuracy as compared to conventional images on analogous types of reconstructions. In fact, several factors influence vessel measurements, even *in-vitro*, with reported differences of 2 mm [25,26]. In human clinical imaging, results are even more discouraging due to notoriously high inter-method, inter-technique, inter-observer and intra-observer differences even for large vessels as the aorta, so high that the latest European guidelines for aortic pathology recommend that only differences of > 5 mm be considered as clinically significant [27,28].

It is important to notice that with K-edge imaging, both K-edge and conventional images, derived from the same acquisition, are available. This means that K-edge images can be employed to accurately assess vessel patency and quantify stenosis, on calcification-free angiographic reconstructions, while conventional images can be used, for instance, to evaluate plaque characteristics.

Although K-edge image quality was inferior to that of conventional images, our results are encouraging and promising. Even more so when considering that conventional and K-edge images derive from the same acquisition but are actually conveying different information so that direct comparison of traditional image quality metrics could be seen as a stretch. In our study, very small vessels are strongly impacted by image noise. However, those with a diameter ≤ 1 mm would have been hardly visible with energy-integrating detectors CT. Noise might have also influenced the concentration values of Gd in the peripheral arteries explaining why they were lower than in the aorta. However, other factors such as the timing of acquisition and partial volume effect may affect these values. It should also be kept in mind that image quality of K-edge images will most likely be ameliorated in the years to come. Whereas in our study we tested only available reconstruction parameters designed for conventional

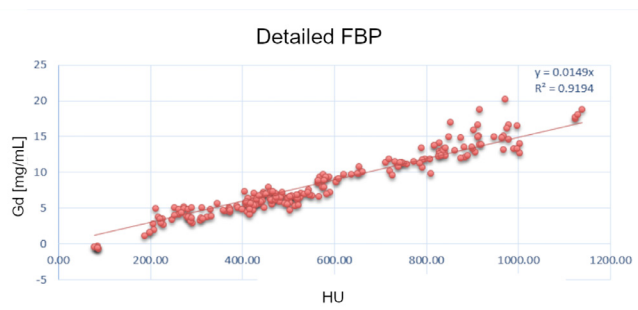


Fig. 6. Correlation of HU and gadolinium (Gd) concentration values in the aorta of the rabbits as measured on conventional and angio-Gd-K-edge images.

images, research on reconstruction parameters, including with artificial intelligence-based algorithms is ongoing [29,30]. Improvements in image quality will certainly allow lowering the dose of contrast material thus reducing the current gap to human use.

Although K-edge imaging offers all the above-mentioned advantages, it does not overcome the need to inject contrast media for vascular applications. Even more constrainingly, the key molecules of the contrast media have to present a K-edge peak at energies detectable by SPCCT. Hence, iodine-based contrast media cannot be employed for K-edge imaging as the value of its peak is 33 keV, too low to be explored. Having to use GBCA is not *per se* a negative news. Indeed, GBCAs have been used daily in clinical routine for many years. It has been recently shown that gadolinium can be detected in intracranial deposits, raising concerns and alertness [31]. However, this was the case only for linear GBCAs and not for macrocyclic ones, such as gadoteridol (ProHance[®], Bracco Imaging) directly tested in the present study, and gadoterate meglumine (Dotarem[®], Guerbet) which is based on the GdF³⁺ cage complex [32].

A major limitation of our study is that the dose of contrast material needed to obtain our results is not compatible with a safe administration in humans. In fact, this dose is about eight times the highest dose recommended for clinical use. This important limitation is likely to be overcome in the next years as it is driving further research to implement new safe molecules and nanoparticles with higher concentration of gadolinium [33]. An example of such new contrast media is one of the GBCAs we tested, GdF3, hybrid nanoparticles with high gadolinium loading and stable inorganic core [9]. These advancements coupled to improvements in image quality, spectral resolution, K-edge material detection and quantification are expected to allow translation of angio-Gd-K-edge in humans. Even bicolor imaging (that is imaging of two contrast media/materials at the same time) might become feasible [34]. Another limitation is that the reduced number of rabbits per type of GBCA prevented us to draw any conclusion about the differences between the two contrast materials.

In conclusion, with SPCCT, angio-Gd-K-edge after intravenous administration of two different GBCAs in rabbits is feasible and allows for angiography-like visualization of very small arteries. In addition, this technique allows reliable measurement of small

Table 3

Hounsfield unit, gadolinium concentration, noise, signal-to-noise ratio and contrast-to-noise ratio per type of reconstruction.

Reconstruction	Conventional				K-edge gadolinium			
	HU	Noise	SNR-HU	CNR-HU	Gd [mg/mL]	Noise	SNR-Gd	CNR-Gd
Soft					8.4 ± 4.3	1.0 ± 0.4	8.7 ± 3.5	11.6 ± 7.0
Soft iDose 3					8.5 ± 4.3	0.9 ± 0.4	9.4 ± 3.9	14.8 ± 9.2
Detailed	569 ± 235	27.7 ± 6.1	21.0 ± 8.8	22.1 ± 10.4	8.3 ± 4.0	2.0 ± 0.5	4.3 ± 2.1	5.1 ± 2.6
Detailed iDose 3	568 ± 234	23.8 ± 6.7	24.7 ± 10.3	21.5 ± 10.2	8.3 ± 4.0	1.7 ± 0.5	5.0 ± 2.4	6.4 ± 3.4

CNR, contrast-to-noise ratio; HU, hounsfield unit; SNR, signal-to-noise ratio.

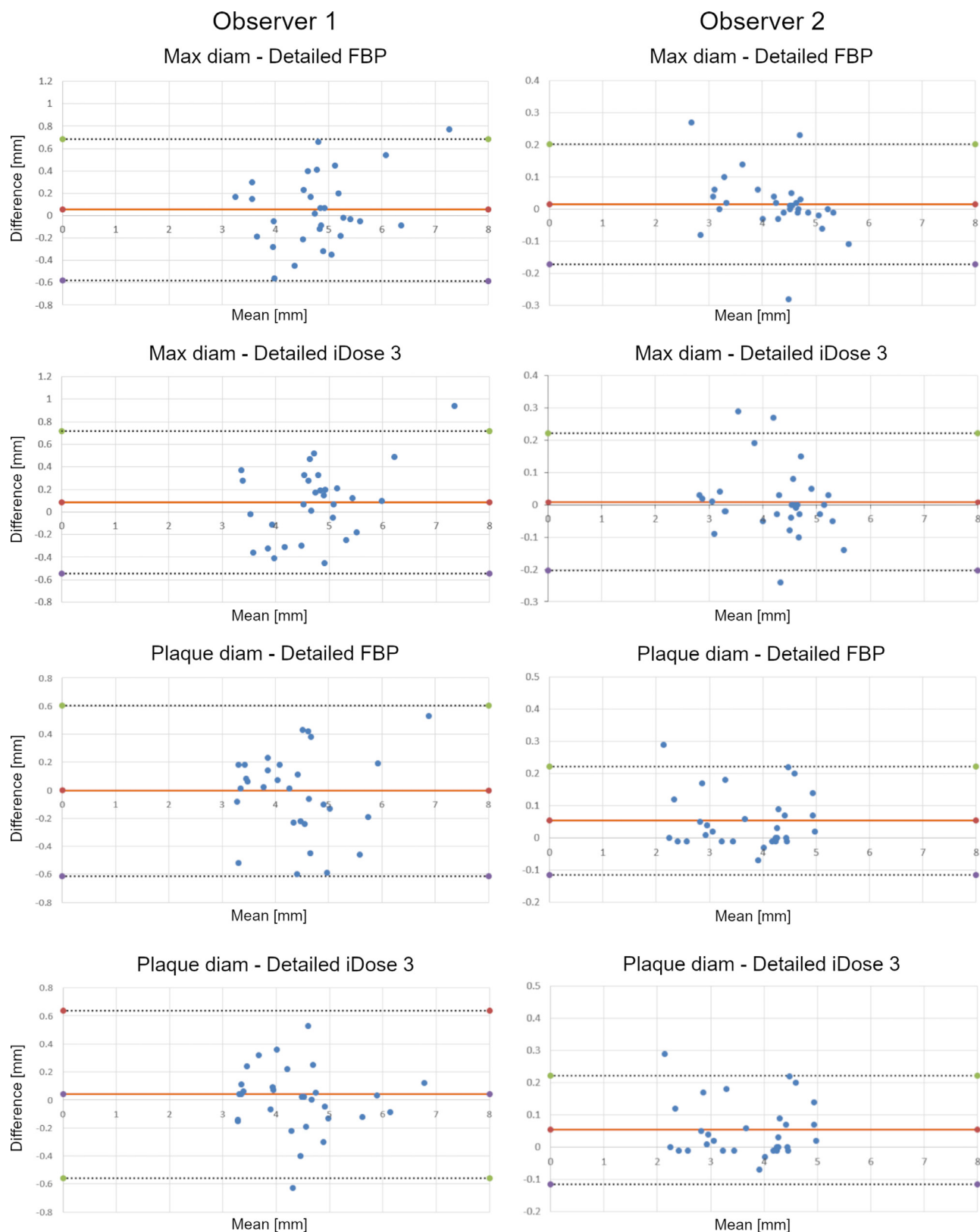


Fig. 7. Bland Altman plots of aortic measurements on conventional vs. angio-Gd-K-edge for the two observers and different reconstructions.

vessels, even for those close to atherosclerotic plaques and bones. However, further research to develop new contrast materials and improve K-edge image quality is needed before this technique can be safely translated in clinical routine.

Human and animal rights

The authors declare that the work described has been carried out in accordance with the Declaration of Helsinki of the World Medical

Association revised in 2013 for experiments involving humans as well as in accordance with the EU Directive 2010/63/EU for animal experiments.

Informed consent and patient details

Not applicable.

Animals right

All procedures were conducted in accordance with the European Directive 2010/63/UE, approved by the Ethics Committee and authorized by the French Ministry of Higher Education, Research and Innovation (APAFIS#27330). All experiments performed after specific approval from the Institutional Animal Care and Use Committee (CELYNE committee, APAFIS#1732-2015091411181645).

Funding

This work was performed within the framework of the EU's H2020 research and innovation program under the grant agreement no. 633937.

Author contributions

All authors attest that they meet the current International Committee of Medical Journal Editors (ICMJE) criteria for Authorship.

Declaration of Competing Interest

Yoad Yagil PhD, Elias Lahoud PhD, Klaus Erhard PhD, Bernhard Brendel PhD and Philippe Coulon PhD are employees of Philips Healthcare.

CRedit authorship contribution statement

Sara Boccalini: Conceptualization, Data curation, Formal analysis, Investigation, Methodology, Validation, Visualization, Writing – original draft, Writing – review & editing. **Riham Dessouky:** Conceptualization, Data curation, Formal analysis, Visualization, Writing – original draft, Writing – review & editing. **Pierre-Antoine Rodesch:** Data curation, Formal analysis, Software, Writing – review & editing. **Hugo Lacombe:** Data curation, Formal analysis, Writing – review & editing. **Yoad Yagil:** Investigation, Project administration, Resources, Software, Writing – review & editing. **Elias Lahoud:** Investigation, Resources, Software, Writing – review & editing. **Klaus Erhard:** Methodology, Resources, Software, Writing – review & editing. **Bernhard Brendel:** Methodology, Resources, Software, Writing – review & editing. **Philippe Coulon:** Resources, Software, Writing – review & editing. **Jean-Baptiste Langlois:** Investigation, Methodology, Resources, Writing – review & editing. **Frederic Chaput:** Investigation, Methodology, Resources, Writing – review & editing. **Stephane Parola:** Investigation, Methodology, Resources, Writing – review & editing. **Loic Bousset:** Conceptualization, Data curation, Funding acquisition, Investigation, Methodology, Project administration, Supervision, Validation, Writing – review & editing. **Frederic Lerouge:** Investigation, Methodology, Resources, Writing – review & editing. **Salim Si-Mohamed:** Conceptualization, Investigation, Methodology, Project administration, Resources, Software, Validation, Visualization, Writing – review & editing. **Philippe C. Douek:** Conceptualization, Data curation, Funding acquisition, Investigation, Methodology, Project administration, Supervision, Validation, Visualization, Writing – review & editing.

References

- [1] Knuuti J, Wijns W, Saraste A, Capodanno D, Barbato E, Funck-Brentano C, et al. 2019 ESC Guidelines for the diagnosis and management of chronic coronary syndromes. *Eur Heart J* 2019;41:1–71.
- [2] Abdulla J, Pedersen KS, Budoff M, Kofoed KF. Influence of coronary calcification on the diagnostic accuracy of 64-slice computed tomography coronary angiography: a systematic review and meta-analysis. *Int J Cardiovasc Imaging* 2012;28:943–53.
- [3] de Laforcade L, Bobot M, Bellin MF, Clément O, Grangé S, Grenier N, et al. Kidney and contrast media: common viewpoint of the French Nephrology societies (SFNDT, FIRN, CJN) and the French Radiological Society (SFR) following ESUR guidelines. *Diagn Interv Imaging* 2021;102:131–9.
- [4] Marchal G, Bosmans H, Van Hecke P, Speck U, Aerts P, Vanhoenacker P, et al. MR angiography with gadopentetate dimeglumine-polylysine: evaluation in rabbits. *AJR Am J Roentgenol* 1990;155:407–11.
- [5] Si-Mohamed SA, Boccalini S, Lacombe H, Diaw A, Varasteh M, Rodesch PA, et al. Coronary CT angiography with photon-counting CT: first-in-human results. *Radiology* 2022;303:303–13.
- [6] Sigovan M, Si-Mohamed S, Bar-Ness D, Mitchell J, Langlois JB, Coulon P, et al. Feasibility of improving vascular imaging in the presence of metallic stents using spectral photon counting CT and K-edge imaging. *Sci Rep* 2019;9:1–9.
- [7] Si-Mohamed S, Bar-Ness D, Sigovan M, Tatar-Leitman V, Cormode DP, Naha PC, et al. Multicolor imaging with spectral photon-counting CT: a phantom study. *Eur Radiol Exp* 2018;2:34.
- [8] Si-Mohamed SA, Sigovan M, Hsu JC, Tatar-Leitman V, Chabalbryse L, Naha PC, et al. In vivo molecular K-edge imaging of atherosclerotic plaque using photon-counting CT. *Radiology* 2021;300:98–107.
- [9] Halttunen N, Lerouge F, Chaput F, Vandamme M, Karpati S, Si-Mohamed S, et al. Hybrid Nano-GdF3 contrast media allows pre-clinical in vivo element-specific K-edge imaging and quantification. *Sci Rep* 2019;9:1–8.
- [10] Steadman R, Herrmann C, Livne A. Nuclear instruments and methods in physics research A ChromAIX2 : a large area, high count-rate energy-resolving photon counting ASIC for a spectral CT prototype. *Nucl Inst Methods Phys Res A* 2017;862:18–24.
- [11] Schlomka JP, Roessl E, Dorscheid R, Dill S, Martens G, Istel T, et al. Experimental feasibility of multi-energy photon-counting K-edge imaging in pre-clinical computed tomography. *Phys Med Biol* 2008;53:4031–47.
- [12] Barat M, Jannot AS, Dohan A, Soyer P. How to report and compare quantitative variables in a radiology article. *Diagn Interv Imaging* 2022;103:571–3.
- [13] Symons R, Cork TE, Lakshmanan MN, Evers R, Davies-Venn C, Rice KA, et al. Dual-contrast agent photon-counting computed tomography of the heart: initial experience. *Int J Cardiovasc Imaging* 2017;33:1253–61.
- [14] Boccalini S, Si-Mohamed S, Dessouky R, Sigovan M, Bousset L, Douek P. Feasibility of human vascular imaging of the neck with a large field-of-view spectral photon-counting CT system. *Diagn Interv Imaging* 2021;102:329–32.
- [15] Si-Mohamed S, Boccalini S, Rodesch P-A, Dessouky R, Lahoud E, Broussaud T, et al. Feasibility of lung imaging with a large field-of-view spectral photon-counting CT system. *Diagn Interv Imaging* 2021;102:305–12.
- [16] Boccalini S, Si-Mohamed S. Spectral photon counting CT: not just a pimped-up new version of dual-energy CT. *Diagn Interv Imaging* 2023;104:51–2.
- [17] Anxionnat R, Bracard S, Macho J, Da Costa E, Vaillant R, Launay L, et al. 3D angiography: clinical interest—first applications in interventional neuroradiology. *J Neuroradiol* 1998;25:251–62.
- [18] Cormode DP, Roessl E, Thran A, Skajaa T, Gordon RE, Schlomka JP, et al. Atherosclerotic plaque composition: analysis with multicolor CT and targeted gold nanoparticles. *Radiology* 2010;256:774–82.
- [19] Boccalini S, Swart LE, Bekkers JA, Nieman K, Krestin GP, Bogers AJ, et al. CT angiography for depiction of complications after the Bentall procedure. *Br J Radiol* 2018;20180226.
- [20] Li P, Xu L, Yang L, Wang R, Hsieh J, Sun Z, et al. Blooming artifact reduction in coronary artery calcification by a new de-blooming algorithm: initial study. *Sci Rep* 2018;8:1–8.
- [21] Fuchs A, Kühl JT, Chen MY, Viladés Medel D, Alomar X, Shanbhag SM, et al. Subtraction CT angiography improves evaluation of significant coronary artery disease in patients with severe calcifications or stents: the C-Sub 320 multicenter trial. *Eur Radiol* 2018;28:4077–85.
- [22] Viladés Medel D, Leta R, Alomar Serrallach X, Carreras Costa F, Pons-Lladó G. Reliability of a new method for coronary artery calcium or metal subtraction by 320-row cardiac CT. *Eur Radiol* 2016;26:3208–14.
- [23] Mannil M, Ramachandran J, Vittoria De Martini I, Wegener S, Schmidt B, Flohr T, et al. Modified dual-energy algorithm for calcified plaque removal: evaluation in carotid computed tomography angiography and comparison with digital subtraction angiography. *Invest Radiol* 2017;52:680–5.
- [24] Tran DN, Straka M, Roos JE, Napel S, Fleischmann D. Dual-energy CT discrimination of iodine and calcium. *Acad Radiol* 2009;16:160–71.
- [25] Suzuki S, Furu S, Kaminaga T, Yamauchi T. Measurement of vascular diameter in vitro by automated software for CT angiography: effects of inner diameter, density of contrast medium, and convolution kernel. *AJR Am J Roentgenol* 2004;182:1313–7.
- [26] Morsbach F, Berger N, Desbiolles L, Poropat T, Leschka S, Alkadhi H, et al. Systematic analysis on the relationship between luminal enhancement, convolution kernel, plaque density, and luminal diameter of coronary artery stenosis: a CT phantom study. *Int J Cardiovasc Imaging* 2013;29:1129–35.
- [27] Bons LR, Duijnhouwer AL, Boccalini S, van Den Hoven AT, van Der Vlugt MJ, Chelu RG, et al. Intermodality variation of aortic dimensions : how, where and when to measure the ascending aorta. *Int J Cardiol* 2018;6–11.

- [28] Erbel R, Aboyans V, Boileau C, Bossone E, Bartolomeo RD, Eggebrecht H, et al. 2014 ESC Guidelines on the diagnosis and treatment of aortic diseases: document covering acute and chronic aortic diseases of the thoracic and abdominal aorta of the adult—the task force for the diagnosis and treatment of aortic diseases of the European. *Eur Heart J* 2014;35:2873–926.
- [29] Rodesch PA, Rebuffel V, Fournier C, Forbes F, Verger L. Spectral CT reconstruction with an explicit photon-counting detector model: a one-step approach. *Phys Med Imaging* 2018;105:1295–302.
- [30] Willemink MJ, Noël PB. The evolution of image reconstruction for CT—from filtered back projection to artificial intelligence. *Eur Radiol* 2019;29:2185–95.
- [31] McDonald RJ, McDonald JS, Kallmes DF, Jentoft ME, Murray DL, Thielen KR, et al. Intracranial gadolinium deposition after contrast-enhanced MR imaging. *Radiology* 2015;275:772–82.
- [32] Choi JW, Moon W-J. Gadolinium deposition in the brain: current updates. *Korean J Radiol* 2019;20:134.
- [33] Yon M, Billotey C, Marty JD. Gadolinium-based contrast agents: from gadolinium complexes to colloidal systems. *Int J Pharm* 2019;569:118577.
- [34] Cosset B, Sigovan M, Boccalini S, Farhat F, Douek P, Boussel L, et al. Bicolor K-edge spectral photon-counting CT imaging for the diagnosis of thoracic endoleaks: a dynamic phantom study. *Diagn Interv Imaging* 2023;104:235–42.